PCCP

A classical-path surface-hopping study of Mu, H and T hot-atom collisions with F_2

Werner Jakubetz,*[a] J. N. L. Connor[b] and Philip J. Kuntz[c]

[a] *Institut für Theoretische Chemie und Strahlenchemie, Universität Wien Währingerstrasse 17, A-1090 Vienna, Austria*
[b] *Department of Chemistry, University of Manchester Manchester, UK M13 9PL*
[c] *Hahn-Meitner-Institut GmbH Glienicker Strasse 100, D-14109 Berlin, Germany*

Received 21st October 1998, Accepted 24th December 1998

The collision dynamics of processes pertinent to the hot-atom chemistry of the hydrogen isotopes Mu, H and T with F_2 are explored using mixed quantum–classical techniques. We use classical-path surface-hopping and pure classical-path multi-surface trajectory methods with a set of 14 coupled potential energy surfaces (PESs) from a diatomics-in-molecules (DIM) model. We compare with results from the standard quasiclassical trajectory (QCT) method applied to the electronic ground state surface of the same DIM model. We compute reaction- and dissociation cross sections for centre-of-mass collision energies ranging from threshold to 20 eV. In order to quantify the notion of electronic non-adiabaticity we introduce various cross sections measuring electronically non-adiabatic processes. We find that non-adiabatic effects give rise to pronounced changes in the dynamics of the Mu + F_2 system. In particular, collision-induced dissociation of F_2 by Mu is an essentially electronically non-adiabatic process, proceeding efficiently by a mechanism involving transitions to excited repulsive PESs. In contrast, QCT calculations on the electronic ground state surface predict vanishingly small Mu + F_2 dissociation cross sections. We also discuss some consequences of this behaviour for simulations of Mu hot-atom chemistry.

I Introduction

The hot-atom chemistry[1–3] of muonium (Mu) is accessible through measurements of muon spin rotation (μSR),[4] which is influenced by processes occurring during the thermalisation of energetic positive muons in gases. The close analogy[5–8] to tritium (T) hot-atom chemistry offers the prospect to study hot-atom isotope effects utilising the exceptionally large T/Mu mass ratio of ≈27 (the mass of Mu is 0.114 u, about one ninth that of H). However, since μSR experiments provide just the highly averaged *yield* (from the fraction of Mu ending up in a diamagnetic molecular environment after a series of collisions), the fate of the muon and the underlying kinetics have to be inferred indirectly. This cannot be done without recourse to models of the energetic collisions occurring in the Mu*(T*) + molecule systems (as usual asterisks indicate translationally hot-atoms), together with considerations of energy transfer in the laboratory coordinate system.[9–11] In order to develop such models, reliable theoretical investigations and simulations of the reactive, dissociative, inelastic and elastic elementary processes are indispensable.

Two opposing aspects of high energy collision dynamics are particularly important to the theoretical treatment. On the one hand, at the high nuclear velocities associated with the hyperthermal range, nuclear motion will be strongly classical in nature, and not too sensitive to details of the potential energy surface (PES). Simple dynamical theories or even kinematic arguments can then provide estimates for dissociation- and reaction cross sections.[12–14] On the other hand, the same high nuclear velocities will cause breakdown of the Born–Oppenheimer (BO) separation in many places, even at strongly avoided crossings between well separated adiabatic PESs.[15] This will result in electronically non-adiabatic behaviour, strong coupling of the nuclear and electronic degrees of freedom, and a pronounced sensitivity to details of the adiabatic PESs involved. In view of its small mass, electronic non-adiabaticity must be of particular concern for collisions involving Mu.

Usually models which take advantage of the classical nature of nuclear motion explicitly or implicitly assume this motion to proceed on a (possibly simplified) single PES.[9,12–14] Yet in the energy range of hot-atom chemistry several electronic states will typically be accessible, and behaviour deduced from an adiabatic assumption may be modified or even completely changed by electronic transitions. The extent of the breakdown of the BO separation and the effects of non-adiabaticity on the cross sections are important considerations for simulations of hot-atom chemistry, and more generally for the theory of high-energy molecular collisions.

The techniques of mixed quantum–classical dynamics,[16,17] (surface hopping[17] and classical path[18] methods), are suitable tools for obtaining quantitative information on electronically non-adiabatic processes at high energies. They are hybrid dynamical techniques, in which the electronic degrees of freedom are treated quantum mechanically, whereas the nuclear dynamics are described by classical mechanics.

In this paper we present a mixed quantum–classical investigation of the collision processes contributing to the hot-atom chemistry of Mu*, H* and T* with F_2, with emphasis on the effects of electronic transitions, and on the isotope dependence of these effects. Although no experimental investigations of Mu* + F_2 reactions have so far been reported, there are four reasons making this an attractive prototype system for a computational study:

(a) The kinetics and dynamics of the corresponding thermal reactions of Mu and H are well characterised, both experimentally[19–26] and computationally.[23,26–29] In particu-

lar this means that there is a set of low energy data which can be used as a reference for the hot-atom case.

(b) Both the dissociation energy of F_2 and the barrier to the $X + F_2$ reaction are relatively small, so that reactive and dissociative processes are readily accessible.

(c) A set of diatomics-in-molecules (DIM)[12,30,31] PESs possessing a number of realistic features is available,[32] comprising 24 electronic states of XF_2.

(d) The $X + F_2$ system is one of the classic benchmark systems of molecular collision dynamics.

Simple prototype systems, in which individual contributions to the overall dynamics and kinetics can be identified and models tested, are a valuable source of information assisting the interpretation or prediction of microscopic and bulk observables, *e.g.* hot-atom yields. In particular, atom + homonuclear diatom collisions like $X + F_2$ have just one reactive and one dissociative channel in addition to the elastic and inelastic channels, thus greatly facilitating the isolation of individual effects. In contrast, for polyatomic molecules the various effects contributing to the hot-atom kinetics may become obscured due to competition and entanglement among a multitude of channels including abstraction and substitution reactions as well as dissociation, fragmentation and ionisation.

We do not attempt to provide a full characterisation of the hot-atom yields expected in the $X^* + F_2$ bulk system, as have been reported for instance for $X^* + H_2$.[10,11] Whereas we expect the reactive and dissociative processes to be reasonably well described in our simulations using a set of semiempirical PESs, it is unlikely that the same will be true for elastic and inelastic differential cross sections, which sensitively determine the energy loss of X* in the laboratory system and thus the overall yields. This is because unlike the H_3 system, for which an accurate global *ab initio* based PES is available,[33–35] the PESs in use for most other reactive systems, including the present one, are generally constructed without detailed consideration of the long-range forces and other factors which influence elastic and inelastic differential cross sections.

The macroscopic channels we consider for $X + F_2$ are

$$Mu + F_2 \rightarrow MuF + F \quad (1a)$$

$$Mu + F_2 \rightarrow Mu + F + F \quad (1b)$$

$$H + F_2 \rightarrow HF + F \quad (2a)$$

$$H + F_2 \rightarrow H + F + F \quad (2b)$$

$$T + F_2 \rightarrow TF + F \quad (3a)$$

$$T + F_2 \rightarrow T + F + F \quad (3b)$$

each of these splitting into an array of detailed channels labelled by the electronic, vibrational and rotational quantum numbers of the reagents and products. At very high energies, additional channels involving charge transfer and ionisation are also open, but these will not be dealt with in detail.

In the present study we first reconsider a previous DIM model,[32] which leads to a modified set of PESs we denote DIM1c. We then use DIM1c to study the isotopomeric processes (1), (2) and (3), using mixed quantum–classical dynamical methods, specifically the 'classical-path surface-hopping' (CPSH) technique in the version formulated by one of us[36] and the 'hemiquantal dynamics with the whole DIM basis' (HWD) method of Amarouche *et al.*[37,38] The range of collision energies varies from reaction threshold up to 20 eV, which is the energy range contributing to experimental Mu* yields.[8] Our calculations assume both collision partners are initially in their electronic ground state.

In order to determine the overall effects of electronic transitions on the cross sections, we juxtapose the surface-hopping data with the results from quasiclassical trajectory (QCT) calculations[39] carried out in a standard fashion on the lowest adiabatic electronic DIM PES. We also compare with single-surface QCT results for the commonly used LEPS (London–Eyring–Polanyi–Sato) PES[12] denoted JOT2 of Jonathan *et al.*[23] Anticipating that details of these ground state PESs will become less important at higher energies, a comparison of the two single-surface results should illustrate to what extent the high energy cross sections are determined by gross features of the potential.

Our focus is on the reaction- and dissociation cross sections, on their energy- and isotope dependence, and on the way in which they are affected and modified by electronic non-adiabaticity. In addition to the 'physical' phenomenon of electronic transitions we investigate how variations in the computational methods influence the results. We also discuss how our findings bear on simulations of hot-atom experiments. We will not deal with the influence of electronic non-adiabaticity on the detailed collision dynamics and on the mechanisms of nuclear rearrangement, nor with the mechanisms of the electronic transitions themselves. These are topics of considerable complexity which will be presented separately.[40]

The remaining sections of this paper are organised as follows: Section II is devoted to computational aspects of our investigations, and we give detailed descriptions of the PESs and of the trajectory and surface hopping techniques employed. In Section III we introduce cross sections measuring the participation of non-adiabatic transitions, which quantify the notion of non-adiabatic effects. Our results are presented in Section IV. A discussion and analysis of our findings is in Section V, and Section VI contains a summary and conclusions.

II Computational details

In this Section we describe the PESs and methods used to calculate the reaction- and dissociation cross sections σ_r and σ_d, respectively, for the processes (1)–(3).

A Potential energy surfaces

For all our multi-surface calculations we used a set of PESs denoted DIM1c. This set is closely related to the DIM1 PES previously employed by two of us,[32] with one modification as described below. Using the *ansatz* of Duggan and Grice (DG),[41] 14 $^2A'$ states of DIM1 were constructed from 14 polyatomic basis functions, which requires a total of 21 diatomic states of F_2, HF, F_2^- and HF^+ (in addition, 10 electronic states of $^2A''$ symmetry are also obtained using this set of diatomic states). The covalent–ionic interaction in the $^1\Sigma^+$ states of HF was included. The single modification leading from DIM1 to DIM1c concerns the two lowest $^1\Sigma_g^+$ states of F_2. Following DG,[41] the coupling between the energetically well separated diabatic states was neglected in DIM1. However, when studying non-adiabatic collisions the neglect of coupling terms surely is an undesirable feature, and hence in the construction of DIM1c this approximation is removed by the explicit inclusion of coupling between the diabatic states. The necessary coupling elements have been derived by Polák[42] (for details of his method see ref. 43 and 44). Most notably, including this coupling removes an artificial conical intersection[45,46] between the two lowest adiabatic potential sheets of XF_2 occurring at an X–F_2 Jacobi angle of about 62°,[32] and transforms it into an avoided intersection. Apart from this, the PESs remain largely unchanged.

In order to illustrate the topography of DIM1c with its 14 adiabatic $^2A'$ potential sheets, two sets of potential curves obtained from one-dimensional cuts through the PESs are

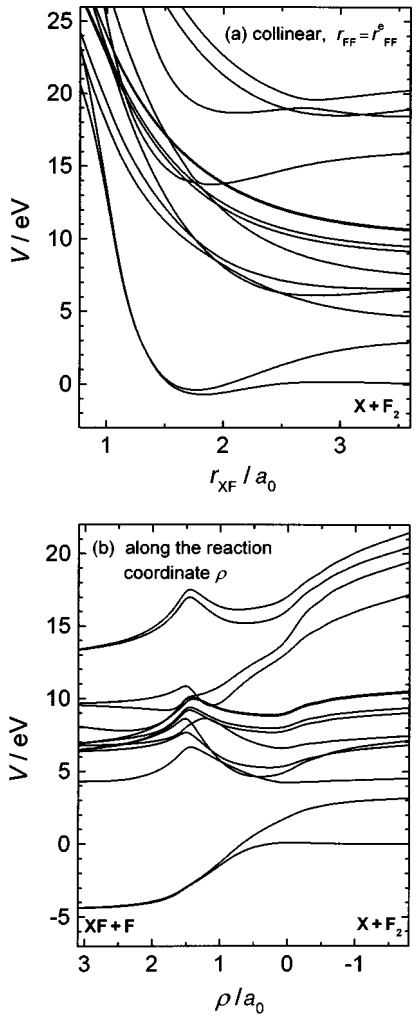

Fig. 1 Collinear cuts through the $X + F_2$ DIM1c adiabatic PESs illustrating the topography of the 14-state system. Note that certain of the potential curves are degenerate in the collinear ($C_{\infty v}$) configuration, and that this additional symmetry gives rise to symmetry-induced conical intersections, apparent as curve crossings. Panel (a): Inelastic channel; cut with r_{FF} fixed at its equilibrium value (r^e_{FF} = 2.67 a_0). Panel (b): Reaction channel; cut along the reaction coordinate ρ (see the text). Here ρ is plotted in the reverse direction so that the asymptotic $X + F_2$ system is towards the right hand side of both panels.

shown in Fig. 1. In the upper panel, the adiabatic potential curves for the collinear approach of X towards F_2 with the bond distance r_{FF} fixed at its equilibrium value of 2.67 a_0 are plotted. These are representative of the adiabatic potentials experienced by the system in non-reactive (inelastic) collisions. The bottom panel provides a similar illustration for reactive encounters, with the cut now taken along the collinear reaction path. The reaction coordinate ρ is defined as the curvilinear coordinate following the (collinear) reaction path on the lowest adiabatic PES, with the origin ($\rho = 0$ a_0) coinciding with the location of the lowest saddle point.

DIM1c has a number of properties that make it a useful tool for the investigation of the reaction and dissociation processes (1)–(3):

(a) In an adiabatic representation it describes 14 low-lying polyatomic (XFF) electronic states of $^2A'$ symmetry and 10 states of $^2A''$ symmetry,

(b) all these states connect asymptotically to diatomic potential curves for F_2, F_2^-, HF and HF^+ taken either from experiment or, in the absence of experimental information, from *ab initio* calculations (see ref. 32), and, except for simplifications in the long-range parts, all asymptotic potential curves agree with spectroscopic or *ab initio* potentials by construction,

(c) couplings between the adiabatic electronic states induced by nuclear motion are readily obtained,

(d) it provides a set of adiabatic surfaces with the correct topology regarding avoided and non-avoided crossings, and at the same time an equivalent diabatic representation useful for the efficient propagation of trajectories,

(e) owing to item (a), the dissociation and ionization energies and the exoergicity of reactions (1a), (2a) and (3a) have the correct experimental values,

(f) the collinear barrier height on the adiabatic ground state PES (0.103 eV) is consistent with the experimental activation energy (0.095 $\pm$ 0.002 eV in the temperature range around 300 K [20]),

(g) QCT calculations using the adiabatic ground state PES[32] yield rovibrational product distributions in gross accord with experimental ones, suggesting that the lowest saddle point and the potential along the reaction path are modeled in a realistic way.

Items (a)–(g) suggest that DIM1c provides a realistic description of the $X + F_2$ system, neglecting only spin–orbit interactions and long-range intermolecular forces. On the other hand, it has long been known that with the standard DIM *ansatz* the global PES of the XF_2 system has shortcomings arising essentially from problems with certain three-body terms.[47] Comparison with *ab initio* calculations [48–51] suggests that a DIM model including ionic structures will possess collinear and slightly non-collinear F–X–F complexes that are too strongly bound on the adiabatic ground state PES. For the collinear case this artificial extra stabilisation gives rise to an underestimate of the height of the ground state barrier, as has been analysed by Last and Baer.[47] For the slightly non-collinear case another consequence is the underestimate of the height of the sideways barrier to reactions (1)–(3), *i.e.* the barrier to reaction by insertion.

In addition to the calculations with the DIM PESs we have also conducted a set of standard (single-surface) QCT calculations using the frequently employed LEPS PES of Jonathan *et al.*[23] designated JOT2. As for the DIM surfaces, the parameters of this semiempirical PES are adjusted with respect to the spectroscopic Morse constants of F_2 and HF, the estimated collinear barrier height and experimental vibrational product distributions. While JOT2 has its own shortcomings, it does not share with DIM1c those described above for F–X–F complexes. By comparing trajectories on the DIM1c adiabatic ground state PES with JOT2, we can estimate to what extent artifacts in the semiempirical models affect the predicted cross sections in the hot-atom regime.

B QCT calculations

For the QCT calculations performed on the adiabatic ground state PES of DIM1c and JOT2, standard Monte Carlo sampling techniques[39] were used to obtain the integral cross sections σ_r and σ_d. In the runs using DIM1c, the required potential derivatives were obtained directly from the Hamiltonian matrix *via* the Hellmann–Feynman theorem.[52,53] The quantisation of F_2 rotation used the convention $J = j\hbar$, where j is the rotational quantum number of F_2 and J is its classical internal angular momentum. The case $j = 0$ is thus represented by a classically non-rotating F_2 molecule.

In each batch the relative translational energy (collision energy) E_T and the vibrational and rotational quantum numbers v and j of F_2 were fixed. E_T was varied in the range 0.5–20 eV, with the initial condition $v = 0$, $j = 0$ used throughout, except for a few additional batches ($v = 0, j = 20$ and $v = 1, j = 0$), which were run in order to investigate the effects of excitation of reagent rotation and vibration on σ_r and σ_d. Batch sizes ranging from 300 to 1000 trajectories were

used, chosen so that the resulting statistical uncertainties were small enough to allow the identification of trends and variations in σ_r and σ_d.

C Classical-path surface-hopping trajectories

For the simulation of electronically non-adiabatic collision processes, our main tool is the CPSH method as formulated and implemented by one of us.[36] In this technique, which draws on classical path and semiclassical theories of molecular scattering from a wide range of sources (*cf.* ref. 37 and 38 and *e.g.* ref. 16–18 and 54–60), the trajectories are started in a pure (adiabatic) electronic state and are then propagated on an effective PES defined as the expectation value of the electronic Hamiltonian, thus taking account of *all* the pure states. As long as there is no non-adiabatic coupling, the system remains in the pure state, just as in the normal surface-hopping procedure.[17,61–66] In a region where the non-adiabatic coupling is significant, the trajectory leads the system into a mixed (superposition) state. If, after traversing the region of non-adiabatic coupling, the system has mixed state character, a 'hop' to a pure adiabatic state is executed, this pure state being selected randomly from the set of all energetically accessible states, each weighted with its population in the mixed state.

The transition to the selected pure state is effected by adding a complex component to each matrix element such that the time evolution of the system reduces the population of all pure state components of the mixed state except that of the desired state. The complex parts of the matrix elements are chosen so that the evolution to the desired state occurs over a short time period, and may indeed be described as a hop. As in standard surface hopping, this procedure also requires a correction to the components of the momenta of each atom in order to accommodate the energy gained or lost in the hop, as detailed further below.

Because we use a DIM model, it is possible to propagate the trajectories efficiently in a well-defined diabatic basis. This is not, however, a necessary prerequisite of the method, and as a check we have also recovered some of the results, albeit in a more time-consuming manner, by propagation in the adiabatic Hamiltonian basis. Of course agreement can only be established at the level of batch averages, since, due to the occurrence of chaos, individual trajectories with given initial conditions may show different outcomes in the adiabatic and diabatic modes.

Non-adiabatic transitions are induced by coupling elements of the form $\langle \dot{\phi}_i | \phi_j \rangle$, where ϕ_i and ϕ_j are time-dependent electronic wavefunctions of the adiabatic states labelled i and j. These elements, or the corresponding expressions in the diabatic basis, are readily obtained as the trajectories are propagated.[36] Our calculations are carried out in a body-fixed coordinate system, and we neglect any coupling between the $^2A'$ and $^2A''$ manifolds of states. This is well justified, since none of the $^2A''$ PESs correlates with the $X\,^1\Sigma_g^+$ state of F_2. Starting from the $^2A'$ ground state PES, transitions to $^2A''$ states will only occur in the asymptotic regions of the F + XF product channel, where they cannot influence the integral cross sections considered in this paper. The set of 14 PESs of $^2A'$ symmetry is used throughout the propagation of the trajectories. Thus in technical terms our CPSH calculations can be characterized as a surface-hopping investigation in a 14-state system, although it is only at the highest energies that all 14 states become energetically accessible and can be reached by surface hops.

A considerable degree of arbitrariness is introduced by the necessary adjustment of the nuclear momenta following a surface hop, and over the years a number of empirical schemes have been proposed to address this point. For most of our results we used a technique (henceforth abbreviated PDOT) in which conservation of total energy is accomplished by readjusting the component of the generalised momentum vector of nuclear motion parallel to the instantaneous acceleration vector.[36] We also used a momentum correction proportional to the non-adiabatic coupling vector (NADC),[64–66] which can be justified by semiclassical arguments[66] and represents a quasi-standard for surface hopping calculations. Finally, we also ran batches applying forced conservation of angular momentum (FCAM).[36] This technique, although more cumbersome to implement, does have considerable 'physical' appeal, guaranteeing that the trajectories obey an essential conservation rule of classical mechanics violated in other methods.

The implementation of a mixed quantum–classical (semiclassical or hemiquantal) theory of electronically non-adiabatic collisions is by no means unique. The range of proposed multistate treatments is marked by surface hopping methods, like Tully's 'molecular dynamics with electronic transitions' (MDET) method,[65] at one end, and by pure classical path (or mean field) methods working with mixed electronic states throughout, *e.g.* the HWD method[36,37] at the other end, and it will depend on the system which of the limiting cases is superior in a given situation.[16] The CPSH method may be described as a hybrid incorporating concepts from both ends. By adjusting certain system parameters it can be pushed towards either end, coinciding with HWD if surface hops are completely suppressed.

Since the choice of propagation method and technique of momentum adjustment may have considerable influence on the subsequent evolution of nuclear motion, it is necessary to critically assess possible choices in order to ascertain that the results obtained are physically significant and do not simply reflect computational strategies. Our principal results have been obtained using the surface hopping mode. Instead of putting forward arguments why this is the preferred method for $X + F_2$ we take a pragmatic point of view: in Section III we will show that global collision attributes are only weakly affected by methodological variations. In particular we find that for σ_r and σ_d there are no pronounced differences between the results from surface hopping and from classical path HWD calculations without surface hops.

The initial conditions and batch sizes for the CPSH and HWD runs are the same as for the single-surface QCT calculations given in Section IIB.

III Cross sections measuring non-adiabatic behaviour

In order to analyse and discuss electronic non-adiabaticity and its signatures in molecular collisions, it is useful to attach a quantitative meaning to notions like 'non-adiabatic effects' and 'the extent of non-adiabatic behaviour'. Some clues about the non-adiabaticity can be obtained from (observable) cross sections for the formation of electronically excited products. However, these provide only indirect and incomplete information about the involvement of non-adiabatic processes in the collision dynamics.

In the following we will introduce measures with the dimensions of [length]^2 that quantify the extent to which electronic coupling and non-adiabatic transitions participate in a collision system (and more specifically in a given process or channel), and how this affects the values of observable cross sections.

A Non-adiabatic corrections $\Delta^{(na)}\sigma_x$

In a pragmatic sense, the effect of electronic non-adiabaticity on a process characterised by a macroscopic or detailed cross section σ_x is the difference between the result of a non-

adiabatic and an adiabatic calculation, *e.g.* between surface-hopping and QCT results, and these two sets of calculations must involve the same electronic ground state PES. Accordingly we define the 'non-adiabatic correction' $\Delta^{(na)}\sigma_x$ by

$$\Delta^{(na)}\sigma_x := \sigma_x^{(na)} - \sigma_x^{(ad)} \quad (4)$$

where the parenthesised superscripts 'na' and 'ad' stand respectively for 'non-adiabatic' and 'adiabatic' and refer to the method of calculation of σ_x (these superscripts will be dropped whenever no confusion may arise). In the following, 'x' is either 'r' or 'd', and CPSH–PDOT and QCT results are used as the 'na' and 'ad' data sets. Positive values of $\Delta^{(na)}\sigma_x$ indicate an enhancement of the process 'x' by electronic transitions, and conversely negative values indicate quenching.

In eqn. (4), $\Delta^{(na)}\sigma_x$ is obtained as the difference of two independently calculated cross sections. However, if identical sets of initial conditions are used for the 'na' and 'ad' batches, a non-adiabatic correction $\Delta^{(na)}P_x$ can be assigned to each single trajectory, which can assume the values 1, 0 and -1, so that $\Delta^{(na)}P_x = 1$ indicates that a trajectory contributes to the process 'x' in the non-adiabatic calculation, but not in the adiabatic one, a value of -1 denotes the reverse case, and $\Delta^{(na)}P_x = 0$ is assigned if the two calculations end up both as 'x' or both as not 'x'. The $\Delta^{(na)}\sigma_x$, can then be determined directly as a weighted batch average of the $\Delta^{(na)}P_x$. Such a strategy helps to reduce statistical uncertainties in the $\Delta^{(na)}\sigma_x$. In the present investigations this 'direct' method was used with CPSH–PDOT and QCT batches set up as described above.

Although $\Delta^{(na)}\sigma_r$ or $\Delta^{(na)}\sigma_d$ let us estimate the applicability or errors of adiabatic calculations in a given situation, they cannot give insight into the origins and evolution of non-adiabatic effects or their interplay with the nuclear dynamics, nor can they be carried over to different initial conditions or different systems without additional analysis.

Electronic coupling and electronic transitions change the potential for nuclear motion, thus influencing the dynamics of individual trajectories and hence, on summing over a batch, they also influence the detailed cross sections and state-, energy- and angular distributions. Yet these effects on individual trajectories need not change the magnitude of integral cross sections because of the possibility of extensive averaging. Thus $\Delta^{(na)}\sigma_x \approx 0$, *i.e.* the absence of a non-adiabatic effect on a cross section, does not rule out electronic non-adiabaticity in the corresponding dynamics.

B Surface-hop cross section σ_{hop}

Ideally a measure of non-adiabaticity would be a cross section which directly monitors electronic transitions, or even electronic coupling, *e.g.* by accounting for all collisions in which transitions occur (and influence the nuclear dynamics). Furthermore it should be consistently defined within the non-adiabatic formalism without requiring a simplistic reference calculation. Such measures can be obtained as batch averages of parameters linked to the evolution of the electronic degree of freedom along individual trajectories run in non-adiabatic mode. With these points in mind, we next define two cross sections measuring the global extent of non-adiabaticity: one based on surface hopping trajectories, the other on classical path trajectories.

The 'surface-hop cross section' σ_{hop} accounts for collisions which involve at least one surface hop off the ground state PES, irrespective of the potential sheet on which the products finally emerge (after further hops, this could be the ground state surface again). In particular for any CPSH batch we determine N_{hop}, the number of trajectories which involve at least one surface hop. N_{hop} is then converted into σ_{hop} in the standard manner,[39] depending on the specific sampling technique used.

In our applications, it is useful to modify the above definition of N_{hop} by omitting all hops between degenerate or near-degenerate potential sheets in the asymptotic ranges of the product channels. This is because these asymptotic transitions have essentially no effect on the nuclear dynamics, nor do they change the values of σ_r or σ_d. It should be noted that the specification of 'near-degenerate' and 'asymptotic' is not unambiguous, and hence the numerical values for σ_{hop} and its components will depend slightly on the criteria chosen. We use a simple geometric criterion and call XF_2 asymptotic if at least two of the interatomic distances are larger than 4.5 a_0.

In fact σ_{hop} is not an integral measure for non-adiabaticity *per se*, but rather for 'sufficiently strong' non-adiabaticity. The definition does not account for collisions in which mixed states evolve in a region of non-adiabatic coupling, but for which no surface hop takes place because the system is sent back to the ground state in the subsequent random transition to a pure state. Averaged over an entire batch, the 'sufficiently strong' non-adiabatic coupling actually monitored by σ_{hop} is approximately equivalent to the formation of a mixed state with at least 50% excited state character.

C Electronic-mixing cross section σ_{mix}

A related indicator of non-adiabaticity, which is sensitive to even the weakest non-adiabatic coupling, can be defined for HWD runs by monitoring along each trajectory the evolution of mixed states. By recording the 'electronic mixing probability' $P_{mix} = \max\{1 - P_1(t)\}$ along a trajectory, *i.e.* the maximum degree of depopulating the electronic ground state [$P_i(t)$ is the time dependent population of the ith electronic state, with the ground state labelled 1], or viewed complementarily, the maximum population of all the excited electronic states, we obtain a measure for the degree of non-adiabatic coupling in individual trajectories. Suitable integration of P_{mix} over a batch leads to the 'electronic-mixing cross section' σ_{mix}, which is an integral measure of *all* non-adiabatic effects, responding even to the weakest non-adiabatic perturbations. This property is particularly useful in the threshold E_T range, where mostly weakly excited mixed states evolve. This means that the hopping probability is small, and due to statistical fluctuations σ_{hop} will have an erratic energy dependence. In this threshold regime σ_{mix} is more informative than σ_{hop} and has a smoother energy dependence.

In the actual determination of σ_{mix} we have again excluded the asymptotic ranges, where the two lowest adiabatic potential sheets are (near-) degenerate. As explained above, we use σ_{mix} mainly in the discussion of threshold non-adiabatic effects. Otherwise it is more consistent to use σ_{hop}, which is obtained from the same batches of CPSH–PDOT trajectories employed for σ_d and σ_r.

D Cross sections for specific channels

Finally, it is also useful to define cross sections which characterise the participation of non-adiabatic coupling for a *specific* process or channel. Such measures can be readily obtained by partitioning σ_{hop} into contributions $\sigma_{hop,x}$, where as above 'x' refers to any macroscopic or detailed process. Below we will consider the dissociative and reactive contributions $\sigma_{hop,d}$ and $\sigma_{hop,r}$ as well as the non-reactive inelastic contribution $\sigma_{hop,i}$. An analogous partitioning can also be defined for σ_{mix}.

IV Results

Our main results are sets of cross sections σ_r and σ_d for the $X + F_2$ collision system, X = Mu, H and T, calculated over an extended energy-range covering the thermal and hot-atom regimes, with E_T ranging from 0.5 to 20 eV (in the centre-of-

mass system). By comparing the mixed quantum–classical calculations with single-surface QCT runs we also obtain σ_{mix} as well as σ_{hop} and its components, which illustrate the role played by electronic non-adiabaticity.

A Reaction- and dissociation cross sections

In Fig. 2 we display σ_r and σ_d for processes (1)–(3) with $v = 0$, $j = 0$. Considering first the effects of non-adiabatic transitions, it is seen that the most remarkable feature is the huge enhancement of σ_d for $Mu + F_2$ upon the inclusion of electronic transitions. On the adiabatic ground state PES of DIM1c and on JOT2, collision-induced dissociation (CID), (1b), is a process of very low probability, while for the heavier isotopes H and T the analogous ground state process provides a very efficient mechanism for F_2 dissociation. If electronic transitions are allowed, this isotope effect in the dissociation cross sections is dramatically reduced, and both the magnitude and the energy-dependence of the CPSH dissociation cross sections for the processes (1b), (2b) and (3b) show only moderate isotopic variations. For the reactive processes (1a), (1b) and (1c), electronic transitions have no pronounced effect on the cross sections, and the reactivities are quite well predicted by single surface QCT simulations. It is also true that the qualitative behaviour of the excitation functions and of the isotope effects are similar for the DIM1c and JOT2 PESs, but as expected there are quantitative differences, and notably differences caused by variations in the PESs clearly exceed those brought about by non-adiabatic coupling.

At higher energies, the ionic channels $X^+ + F_2^-$, $XF^+ + F^-$ and $X^+ + F^- + F$ are open and therefore the PESs asymptotically connected to these states can be populated by electronic transitions. However, such transitions are extremely infrequent, and in all our batches we observed just one trajectory producing $T^+ + F^- + F$ (at $E_T = 16$ eV) and one trajectory producing $HF^+ + F^-$ (at $E_T = 20$ eV). This means that from threshold to $E_T = 20$ eV, the cross sections for formation of ionic products are at most of the order of 0.1 a_0^2 for $T + F_2$, and still smaller for $Mu + F_2$ and $H + F_2$. These small contributions have been included in the σ_r and σ_d shown in Fig. 2.

It should be noted that some products may end up as quasibound molecules, *i.e.* as strongly vibrating/rotating XF or F_2 entities bound only by a centrifugal barrier. We count all such trajectories as dissociative, assuming an experimental setup where the lifetimes of the quasibound molecules are much shorter than the detection time, so that dissociation will have occurred by the time the products are detected. The contribution of quasibound products to σ_d is almost negligible in $Mu + F_2$, but for $T + F_2$ it can reach as much as 10% at some energies.

Tables 1 and 2 contain more detailed results for $E_T = 6$ and 12 eV. These data are given in order to establish the significance of the cross sections in Fig. 2, both for a lower energy (6 eV), where only a few electronic states are accessible, and for a higher one (12 eV), where almost the full array of electronic PESs may contribute. The statistical errors in the results are indicated by the standard deviations of the cross sections. In addition, these comparisons address the sensitivity of the results to the computational technique and to the choice of rovibrational reagent states.

Table 1 demonstrates the degree of consistency and 'convergence' of the cross sections with respect to the propagation methods and to the momentum correction techniques. At both E_T, the different techniques used within the CPSH method have almost no effect on the predicted flow into the macroscopic product channels, and hence on the calculated values of σ_r and σ_d. It should be noted that more sizeable variations are observed for state-resolved cross sections, and therefore it will be necessary to consider carefully the choice of technique if detailed collision attributes like internal product state distributions and differential cross sections are required. It is hardly surprising that such detailed quantities are sensitive to any local repartitioning of momentum among different modes of nuclear motion.

It is also evident in Table 1 that there are only small differences in the cross sections calculated by the CPSH and HWD methods, and this finding is independent of E_T. The results for the H and T systems are virtually identical; however, for these isotopes the inclusion of non-adiabatic coupling has only a small effect on the observed cross sections, and this insensitivity to the method of propagation is not unexpected. Yet even in the case of $Mu + F_2$, where non-adiabatic effects are very important, the differences between the CPSH and HWD cross sections are fairly small.

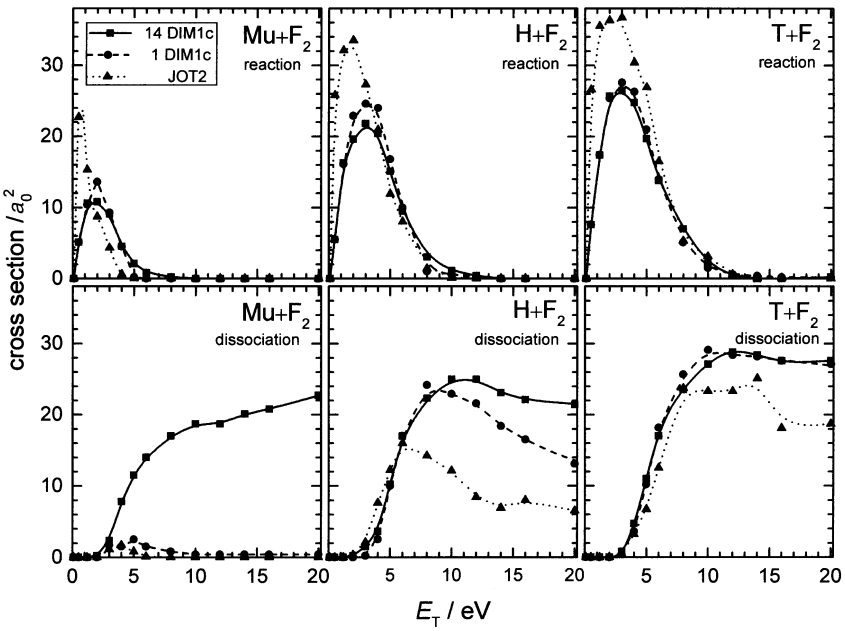

Fig. 2 Reaction- and dissociation cross sections σ_r and σ_d for $X + F_2$ (X = Mu, H, T) *vs.* E_T. (—■—): CPSH–PDOT results for DIM1c (14 coupled PESs). (– – ● – –) QCT results for DIM1c (lowest adiabatic PES). (· ·▲· ·) QCT results for LEPS JOT2 (lowest adiabatic PES). Standard deviations are $\leqslant 1.8$ a_0^2 for all data shown. Owing to the use of different batch sizes, some results differ from the corresponding entries in Tables 1 and 2.

Table 1 $X + F_2(v = 0, j = 0)$ reaction- and dissociation cross sections/a_0^2 obtained with different non-adiabatic propagation techniques

		CPSH–PDOT[a]		CPSH–NADC[b]		CPSH–FCAM[c]		CP HWD[d]	
X	E_T/eV[e]	σ_r[f]	σ_d[g]	σ_r[f]	σ_d[g]	σ_r[f]	σ_d[g]	σ_r[f,h]	σ_d[g,h]
Mu	6	0.9 ± 0.3	13.8 ± 1.2	0.8 ± 0.3	13.5 ± 1.2	1.1 ± 0.4	15.0 ± 1.2	0.3 ± 0.2 (0.3 ± 0.3)	17.9 ± 1.3 (20.6 ± 1.3)
	12	0[i]	18.4 ± 0.8	0[i]	18.2 ± 1.3	0[i]	20.1 ± 1.3	0_i (0^i)	23.3 ± 1.4 (27.1 ± 1.4)
H	6	10.1 ± 1.0	16.0 ± 1.2	9.3 ± 1.0	17.2 ± 1.3	9.2 ± 1.0	17.4 ± 1.3	9.0 ± 1.0 (8.2 ± 0.9)	16.8 ± 1.3 (18.8 ± 1.3)
	12	0.8 ± 0.5	23.0 ± 2.1	0.8 ± 0.5	21.7 ± 2.0	0.4 ± 0.3	24.8 ± 1.8	0.1 ± 0.1 (0.1 ± 0.1)	24.7 ± 1.4 (26.5 ± 1.4)
T	6	13.0 ± 1.1	16.9 ± 1.3	13.4 ± 1.2	16.7 ± 1.3	13.6 ± 1.2	16.9 ± 1.3	13.2 ± 1.2 (12.5 ± 1.2)	16.7 ± 1.3 (17.9 ± 1.3)
	12	0.8 ± 0.5	28.0 ± 2.2	1.3 ± 0.6	27.5 ± 2.2	1.0 ± 0.3	27.5 ± 1.4	0.5 ± 0.3 (0.5 ± 0.3)	28.4 ± 1.4 (29.0 ± 1.4)

[a] DIM1c 14-state classical path surface hopping propagation with momentum adjustment proportional to the time derivative of the generalized momentum vector (PDOT). [b] DIM1c 14-state classical path surface hopping propagation with momentum adjustment proportional to the non-adiabatic coupling vector (NADC). [c] DIM1c 14-state classical path surface hopping propagation with forced conservation of angular momentum (FCAM). [d] DIM1c 14-state classical path HWD propagation (without surface hopping). [e] Translational reagent energy. [f] Reaction cross section (excluding quasibound products). [g] Dissociation cross section (including quasibound products). [h] First entries are from a product analysis carried out directly on the final (mixed) states, entries in parentheses include a correction for mixed states with both dissociative and inelastic contributions (see the text). [i] No reactive trajectories observed.

In HWD, as in all classical path treatments without explicit surface hopping, the system will usually end up in a mixed state, and it is common practice to perform the product analysis directly on this mixed state. There are several well documented problems associated with this situation,[16,37,60,65,67–69] both conceptually and with respect to the technical analysis when the final mixed state has contributions from different macroscopic channels, *e.g.* both from non-dissociative and dissociative molecular product states. In the HWD treatment of $X + F_2$ such a situation prevails, and the problems are both amplified and alleviated by the fact that *all* excited states of F_2 are either repulsive states or, with the single exception of the $^3\Pi_u$ state, are so weakly bound that dynamically they behave like repulsive states. Therefore most trajectories classified as inelastic will in fact have ended up in a superposition state possessing both a non-dissociative component from the contribution of the ground state and a dissociative one from all excited states participating in the mixed state.

An additional contribution to σ_d can thus be estimated from the total population of excited states in all final mixed states assigned as inelastic (and an analogous correction can be made for reactive collisions). Cross sections corrected in this way for HWD are included in Table 1 as the values shown in brackets. The corrections reflect the importance of electronic transitions and show a clear isotopic trend. While the corrections are almost negligible for $T + F_2$, they amount to about 15% of the uncorrected values of σ_d for the Mu system. With this correction applied, the HWD dissociation cross sections for process (1b) are also somewhat larger than the corresponding CPSH ones. Notwithstanding these differences in the numerical values, all qualitative features in the cross sections remain unchanged, irrespective of the choice of HWD or CPSH or of any of their specific implementations. In view of this insensitivity of the cross sections to the computational techniques it can be assumed that the observed effects are indeed due to electronic non-adiabaticity, and their discussion can be based on a single set of results. In particular, the analysis in Section V will use the set of CPSH–PDOT data.

We next consider the effects of varying the F_2 rovibrational state. Table 2 shows that in all methods σ_r and σ_d are fairly insensitive to rotational and vibrational excitation of F_2. The absence of sizeable rotational effects on the $X + F_2$ reaction cross sections has already been well documented for the thermal regime.[23,26,29,32] In these essentially direct impulsive collisions the rotational motion of F_2 is virtually arrested on the collisional timescale, and this behaviour must be further reinforced at high E_T, where the collision times are still shorter.

Finally we find that F_2 vibrational excitation gives rise to only small changes in the H and T cross sections barely outside the statistical uncertainties, and the corresponding effects are even smaller for Mu. Taken together, these results

Table 2 $X + F_2(v, j)$ reaction- and dissociation cross sections/a_0^2 at $E_T = 6$ eV

		DIM1c 14-state CPSH–PDOT[a]		DIM1c 1-state QCT[b]		JOT2 1-state QCT[b]	
X	(v, j)[c]	σ_r[d]	σ_d[e]	σ_r[d]	σ_d[e]	σ_r[d]	σ_d[e]
Mu	(0, 0)	0.9 ± 0.3	13.8 ± 1.2	0[f]	1.4 ± 0.4	0[f]	0.8 ± 0.3
	(0, 20)	0.8 ± 0.5	13.9 ± 1.7	0[f]	1.1 ± 0.5	0[f]	0.4 ± 0.2
	(1, 0)	1.3 ± 0.5	14.6 ± 1.5	0[f]	1.7 ± 0.6	0[f]	0.7 ± 0.2
H	(0, 0)	10.1 ± 1.0	16.0 ± 1.2	9.8 ± 1.0	17.2 ± 1.2	6.7 ± 0.7	14.1 ± 0.9
	(0, 20)	9.3 ± 1.3	16.8 ± 1.6	8.9 ± 1.3	17.8 ± 1.6	5.7 ± 0.6	13.7 ± 0.9
	(1, 0)	7.8 ± 1.2	19.1 ± 1.7	8.1 ± 1.2	19.9 ± 1.7	7.7 ± 0.8	15.6 ± 0.9
T	(0, 0)	13.0 ± 1.1	16.9 ± 1.3	13.9 ± 1.2	16.9 ± 1.3	17.7 ± 1.0	12.5 ± 0.8
	(0, 20)	12.9 ± 1.5	19.1 ± 1.7	12.9 ± 1.5	19.5 ± 1.7	17.7 ± 1.0	13.7 ± 0.9
	(1, 0)	11.5 ± 1.4	19.5 ± 1.7	11.5 ± 1.4	20.8 ± 1.7	16.9 ± 1.0	15.3 ± 0.9

[a] Classical path surface hopping propagation with momentum adjustment proportional to the time derivative of the generalized momentum vector (PDOT). [b] Standard quasiclassical trajectories on the lowest adiabatic PES. [c] Vibrational–rotational quantum numbers of reagent F_2. [d] Reaction cross section (excluding quasibound products). [e] Dissociation cross section (including quasibound products). [f] No reactive trajectories observed.

mean that the cross sections for the specific reagent condition $v = 0$, $j = 0$ are representative for high energy collisions in X + F_2. In particular this conclusion will also hold for simulations of yield experiments, in which energetic X* particles are slowed down in the *thermal* environment of a moderator gas, consisting of molecules in low vibrational states ($v = 0$, 1 in the case of F_2).

B Non-adiabatic behaviour

We will now use the cross sections defined in Section III to analyse the effects of electronic coupling and electronic transitions in the X + F_2 systems. All values for the non-adiabatic corrections and surface hop cross sections reported below were obtained from the data in Fig. 2. The standard deviations in σ_{hop} and its components, and in $\Delta^{(na)}\sigma_r$ and $\Delta^{(na)}\sigma_d$ are $\leqslant 1.8\ a_0^2$. The σ_{mix} were obtained from smaller HWD batches (with a batch size of 100) run specifically for this purpose. The associated standard deviations are $\leqslant 2.4\ a_0^2$ in general, but near threshold the statistical errors are smaller than those for σ_{hop}.

It is instructive to first establish the extent of non-adiabatic behaviour before discussing its effect on the cross sections. To this end, Fig. 3 shows the E_T dependence of σ_{hop}, and in Fig. 4 we augment the low E_T data for σ_{hop} by the analogous results for σ_{mix}. The plots of σ_{hop} *vs.* E_T reveal an effective threshold for electronic transitions around 1 eV, varying with the mass of X in the order Mu < H < T. The contrasting smooth increase of σ_{mix} from $E_T = 0$ eV is shown in Fig. 4. A comparison of Figs. 3 and 4 illustrates the effect of neglecting *weak* non-adiabatic coupling. Notice that for both σ_{hop} and σ_{mix} electronic non-adiabaticity remains negligible at thermal energies. Even at $E_T = 0.5$ eV, well into the range of hyperthermal energies, σ_{mix} is 0.7 ± 0.3, 0.6 ± 0.3 and 0.3 ± 0.1 a_0^2 for Mu, H, and T + F_2, respectively, at least an order of magnitude smaller than the corresponding σ_r.

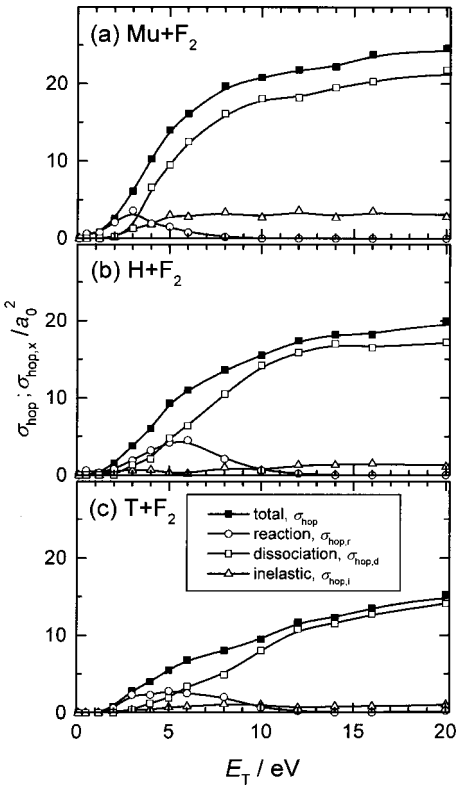

Fig. 3 Electronic non-adiabaticity in the X + F_2 system. E_T dependence of the surface hop cross sections σ_{hop}, and their partitioning into the dissociative, reactive and inelastic contributions $\sigma_{hop,d}$, $\sigma_{hop,r}$ and $\sigma_{hop,i}$. Panel (a): X = Mu. Panel (b): X = H. Panel (c): X = T. All data are from CPSH–PDOT calculations.

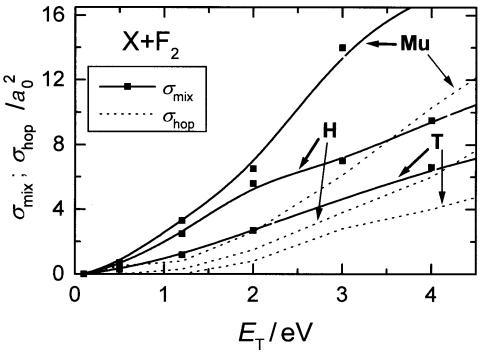

Fig. 4 Electronic non-adiabaticity in the X + F_2 system. E_T dependence of the electronic mixing cross sections σ_{mix} for X = Mu, H and T (from HWD calculations) are shown as full lines for $E_T \leqslant 4.5$ eV. For comparison, smoothed surface hop cross sections σ_{hop} (from CPSH–PDOT calculations) are shown as dotted lines. For $E_T > 4$ eV the corresponding curves for $\sigma_{mix}(E_T)$ and $\sigma_{hop}(E_T)$ run approximately parallel.

In the post-threshold range, σ_{hop} (and σ_{mix}) increase monotonically with E_T, although with different slopes for the different isotopomeric systems. At very high E_T they appear to level off. The high-energy limit of σ_{hop} is only slightly isotope dependent, with values between 20 and 25 a_0^2 (at $E_T = 50$ eV, the values are 24.5, 23 and 21 a_0^2, respectively, for Mu, H and T + F_2, all $\pm 1.8\ a_0^2$). Thus at higher E_T the participation of non-adiabatic processes is of a similar order of magnitude for all three isotopomeric systems. This is in contrast to the dramatically different response to electronic excitation for Mu, H and T CID, with a strong enhancement of σ_d for Mu + F_2 and a near-absence of non-adiabatic effects for T + F_2. In interpreting these high-energy results, it should be noted that for $E_T > 20$ eV, the PESs are obtained by a somewhat arbitrary exponential extrapolation without recourse to concrete data points. Still, it is expected that the qualitative aspects of our findings are not sensitive to such ambiguities.

V Discussion

Having established the extent to which non-adiabatic transitions occur and the effects they have on the cross sections, we next investigate the relation between them, *i.e.* we relate σ_{hop} and its components to $\Delta^{(na)}\sigma_r$ and $\Delta^{(na)}\sigma_d$. From Section III it is clear that, at least at the level of integral cross sections, the different isotopomeric systems and the different macroscopic rearrangement processes respond differently to non-adiabatic transitions: Thus T + F_2 is less sensitive to electronic non-adiabaticity than is Mu + F_2, and reaction shows less sensitivity than dissociation. On the other hand, Fig. 3 shows that electronic transitions are common for all isotopes, and that the insensitivity of certain integral cross sections to electronic transitions cannot be due to the *absence* of such events. It then follows that non-adiabatic transitions are just not effective for influencing the magnitudes of σ_d and σ_r in these cases.

A Reaction

For reactive collisions, a visual comparison of the CPSH and QCT results in Fig. 2 suggests that non-adiabatic processes do not have a pronounced effect on the σ_r for any of the isotopomeric systems. Fig. 5 shows indeed that not just in the thermal range, but across the entire range of peak reactivity the correction term $\Delta^{(na)}\sigma_r$ is much smaller in magnitude than σ_r itself. However, even though the $\Delta^{(na)}\sigma_r$ are small, their E_T dependence follows a distinct pattern, common to the three isotopomeric reactions (1a), (2a) and (3a), and clearly recognisable in Fig. 5. Near threshold and across the range of high reactivity, electronic transitions tend to quench reaction

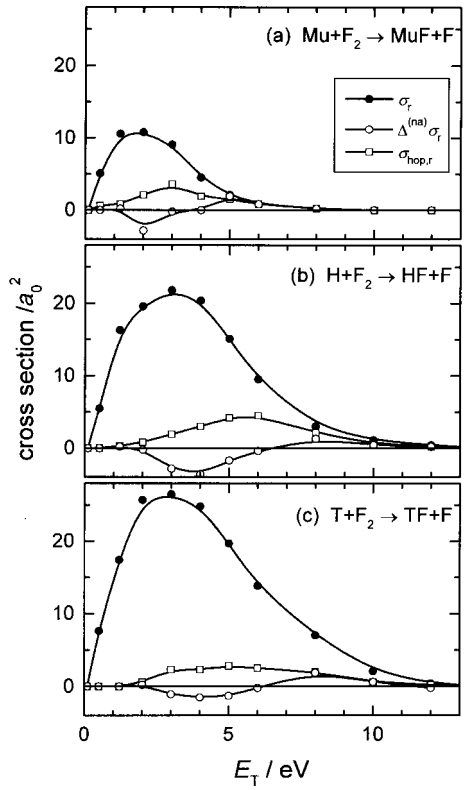

Fig. 5 Cross sections for non-asymptotic electronic transitions in X + F_2 reactions *vs.* E_T. The reactive contributions to the surface hop cross sections, $\sigma_{hop,r}$ (□), and the non-adiabatic corrections to the reaction cross sections, $\Delta^{(na)}\sigma_r$ (○), are superimposed on the CPSH–PDOT reaction cross sections σ_r (●). Panel (a): X = Mu. Panel (b): X = H. Panel (c): X = T. Standard deviations are $\leqslant 1.8\ a_0^2$ for all data points.

weakly, as indicated by the negative values of $\Delta^{(na)}\sigma_r$. At higher E_T this trend is reversed, and weak non-adiabatic enhancement of the reaction is observed throughout the tail of the excitation functions.

Since non-adiabatic coupling affects σ_r in opposing ways for different E_T ranges, it is necessary to estimate the integrated effects on the reactivity in bulk systems characterised by thermal or non-thermal energy distributions. Thermal-average reaction rate coefficients will be slightly reduced by non-adiabatic effects because of the decrease of σ_r in the lower E_T range. In contrast, a non-adiabatic *enhancement* of thermal rate coefficients would require RT to be pushed well into the range of non-adiabatic enhancement of σ_r, which would correspond to $T > 60\,000$ K.

Hot-atom reactions are not properly characterised by thermal reagent distributions. A semi-quantitative tool for assessing the overall reactivity in hot-atom reactions is provided by the reactivity integral I of Wolfgang–Estrup theory,[9,70]

$$I = \frac{1}{\sigma_{max}} \int_{E_{min}}^{E_{max}} \frac{\sigma_r(E_T)}{E_T}\, dE_T \qquad (5)$$

The scaling factor σ_{max} is the total geometrical cross section. Since we are only interested in relations between the adiabatic and non-adiabatic results, explicit values for σ_{max} are not required. We take E_{min}, the onset of hot-atom reactions, at 1 eV,[6] and the choice of the upper integration limit E_{max} is apparent from the excitation functions in Fig. 5.

For all isotopomeric reactions, we find that on replacing QCT cross sections by CPSH–PDOT ones, I decreases by just a few (1–9) percent, which corresponds to changes almost within the statistical error limits. Due to the large uncertainties, no clear isotopic trends can be identified. Thus the contribution of non-adiabatic effects to simulated hot-atom yields is of minor importance. In comparison, the QCT data for LEPS JOT2 show that the changes caused by variations in the PES may greatly exceed these direct non-adiabatic effects.

On the other hand, indirect contributions from non-adiabatic effects in the energy transfer cross sections which affect the slowing down of Mu* may be more important than the direct ones. In general, since additional collision energy can be absorbed by electronic excitation, energy loss mechanisms will tend to be underestimated in purely adiabatic (QCT) computations. Hence allowing for electronic non-adiabaticity, a more efficient slowing down of X is expected for all isotopomeric systems.

We now consider the *participation* of electronic transitions in reactive collisions, as opposed to their net effect on σ_r. For E_T below ≈ 5 eV, we find $\sigma_{hop,r} \ll \sigma_r$, implying that surface hops in non-asymptotic regions of the PESs occur only in a small fraction of the reactive trajectories. At the same time it follows from the small, but negative values of $\Delta^{(na)}\sigma_r$ that non-adiabatic processes slightly suppress reaction, *i.e.* some trajectories which are reactive if propagated adiabatically on the ground state PES change their macroscopic course following a surface hop and turn non-reactive. For $E_T > 5$ eV, the fraction of non-adiabatic trajectories contributing to reaction becomes more significant, and for Mu the reaction eventually becomes entirely non-adiabatic in the high E_T tail of the excitation function.

In addition, extensive non-adiabatic coupling is observed in the XF + F product channel, where the two lowest PESs are (near-) degenerate. As noted in Section III, for our model asymptotic transitions have no effect on σ_r. However, such processes would become relevant if spin–orbit splittings were included.

B Collision induced dissociation

It has already been pointed out in Section IIA that the excited electronic states of F_2 are repulsive. This implies that in the non-reactive channel all excited XFF PESs are asymptotically repulsive, and thus dissociation can be induced by electronic transitions. In fact dissociation is inevitable if there is no transition back to the ground state. Since the probability of electronic transitions increases with E_T, more trajectories which are inelastic if propagated on the ground state PES will become dissociative if surface hopping is included.

Fig. 6 illustrates the relations between electronic transitions and the CID processes (1b), (2b) and (3b). For Mu + F_2, the amount of dissociation in electronically adiabatic collisions on the ground state PES is almost negligible: electronic transitions are a prerequisite for dissociation. This can be seen from the fact that $\Delta^{(na)}\sigma_d$, $\sigma_{hop,d}$ and σ_d are nearly identical throughout the E_T range considered.

Obviously dissociation of F_2 by Mu is essentially an electronically non-adiabatic process. It is less obvious whether conversely CID by T should be viewed as an electronically adiabatic process. Although it is true that $\Delta^{(na)}\sigma_d \approx 0$ for all E_T in Fig. 6(c), and that QCT calculations on the ground state PES thus yield the correct values of σ_d, the sizeable values of $\sigma_{hop,d}$ indicate that electronic transitions do in fact occur in a significant fraction of the dissociative collisions; *e.g.*, at E_T = 20 eV surface hops are observed in $\approx 50\%$ of all dissociative trajectories.

Over the entire E_T range considered, dissociation of F_2 by T occurs both by an adiabatic and a non-adiabatic mechanism. Hence the dissociation process (3b) cannot be classified as electronically adiabatic, although from a pragmatic point of view simulations may be carried out in a purely adiabatic mode if total dissociation cross sections or rate coefficients are the only quantities of interest. However, while the macroscopic outcome of these collisions is not affected by the

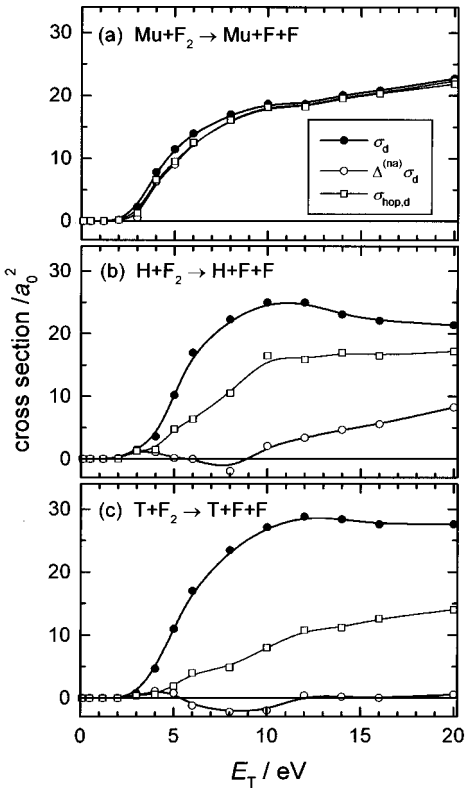

Fig. 6 Cross sections for non-asymptotic electronic transitions in X + F_2 collision-induced dissociation *vs.* E_T. The dissociative contributions to the surface hop cross sections, $\sigma_{hop,d}$ (□), and the non-adiabatic corrections to dissociation, $\Delta^{(na)}\sigma_d$ (○), are superimposed on the CPSH–PDOT dissociation cross sections σ_d (●). Panel (a): X = Mu. Panel (b): X = H. Panel (c): X = T. Standard deviations are $\leqslant 1.8\ a_0^2$ for all data points.

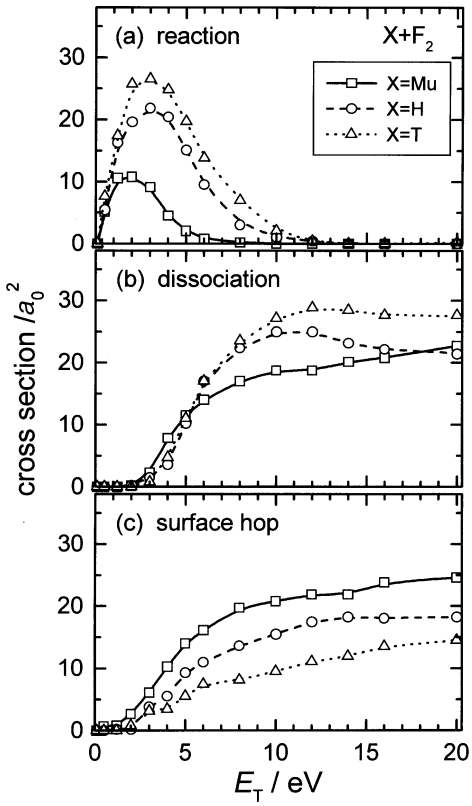

Fig. 7 Isotope dependence of X + F_2 cross sections *vs.* E_T. Panel (a): Reaction cross sections σ_r. Panel (b): Dissociation cross sections σ_d. Panel (c): Surface hop cross sections σ_{hop}. (—□—) X = Mu. (– –○– –) X = H. (··△··) X = T. All data are CPSH–PDOT results for DIM1c. Standard deviations are $\leqslant 1.8\ a_0^2$ for all data points.

surface hops, it must be expected that detailed observables, *e.g.* the angular distributions of the scattered T atoms, will be altered.

From Fig. 6(b) it would appear that process (2b) represents an intermediate case. For $E_T < 9$ eV, H behaves like T, inasmuch there is no systematic non-adiabatic enhancement of dissociation. At higher E_T, $\Delta^{(na)}\sigma_d$ starts to increase and the mechanism gradually switches to the one observed for Mu, where the dissociation of F_2 requires triggering by electronic transitions. However, a full picture of the mechanism and the isotopic variations emerges only if an even more extended range of E_T is considered. This will be demonstrated in Section VC.

C Isotope dependence of σ_r and σ_d

In Figs. 7(a) and (b), the CPSH–PDOT cross sections σ_r and σ_d are plotted in a form that illustrates their isotope dependence. For comparison, in Fig. 7(c) we also show the same information for σ_{hop}.

Generally, the isotope dependence of the excitation functions $\sigma_r(E_T)$ and $\sigma_d(E_T)$ is not spectacular, with the reactive channel showing the more distinctive isotope effect. The excitation functions for reactions (1a), (2a) and (3a) in Fig. 7(a) all have the same shape, but with increasing mass m_X of X the reactivity increases and both the maximum of σ_r and the cutoff are shifted to higher E_T values. As expected from the mass ratios, this effect is more pronounced for the Mu/H pair than for H/T.

The isotopic variations in the σ_d for the processes (1b), (2b) and (3b) in Fig. 7(b) are very moderate. For each of the isotopes, σ_d rises steeply from the effective dissociation threshold at $E_T \approx 3$ eV up to $E_T \approx 10$ eV and then appears to level off at a value in excess of 20 a_0^2.

More remarkable are the different roles of electronic transitions in establishing the isotopic variations. The isotope dependence of σ_r is not directly related to non-adiabatic behaviour, since Fig. 2 shows that the QCT $\sigma_r^{(ad)}$ exhibit similar isotope effects. In sharp contrast, the fact that the isotope dependence of σ_d is only weak *is the result* of electronic non-adiabaticity, since the QCT $\sigma_d^{(ad)}$ show a very pronounced isotope dependence. This means that in CID of F_2 by Mu, H, and T, the same apparent behaviour is brought about by entirely different mechanisms. This interesting situation is best analysed in two steps: we will first consider the adiabatic results, and this will be followed by a discussion of the extent and effects of non-adiabaticity.

We first discuss $\sigma_r^{(ad)}$ and $\sigma_d^{(ad)}$ from the QCT calculations. Although the results in Fig. 2 seem to suggest otherwise, on the adiabatic ground state PES the six processes (1)–(3) have a common mechanism, which emerges if the translational velocity v_T (or the collision time $\tau_c = l_c/v_T$, where l_c is a characteristic length of the system), rather than E_T, is used as the independent variable. The description of the mechanism in terms of τ_c is particularly suggestive, since τ_c can be interpreted as the duration the system spends as a strongly interacting collision complex, in which the different modes of nuclear motion are coupled by the PES. The higher v_T (and hence E_T) or the smaller m_X, the shorter is τ_c, so that less time is available to build up linear momentum in the direction of F–F (or F–FX) translational motion as the time-integrated force exerted by the potential,[6,12] and the less likely is the separation of the F atoms, *i.e.* reaction or dissociation. Therefore the isotopomeric $\sigma_r(E_T)$ and $\sigma_d(E_T)$ all have the same single peaked shape brought about by the interplay of a post-threshold increase and a decrease caused by the kinematic E_T cutoff. At any fixed E_T in the post-threshold range, this implies an isotope dependence favouring reaction and dissociation in T + F_2 over H + F_2 and Mu + F_2.

This kinematic argument is *quantitatively* valid for the case of dissociation, with one modification described below: for sufficiently high v_T, $\sigma_d^{(ad)}(v_T)$ is a decreasing function of v_T and is isotopically invariant. This is demonstrated in Fig. 8, where $\sigma_d^{(ad)}$ is shown as a function of u_T, an *effective* translational velocity defined by

$$u_T = [2(E_T + \Delta E_T)/\mu_{X,F_2}]^{1/2} \quad (6)$$

which differs from the *asymptotic* translational velocity v_T due to the inclusion of ΔE_T. This energy increment accounts for the attractivity of the XF_2 PES, which causes the system to assume a slightly higher translational energy during a close collision. The results in Fig. 8 use $\Delta E_T = 3$ eV, which provides the best agreement of the isotopic $\sigma_d^{(ad)}$ at high u_T, but this choice is not crucial to the argument.

If applied to *reaction* on the ground state PES, the kinematical argument is valid qualitatively, but due to additional dynamical contributions no true isotopic invariance is obtained for $\sigma_r^{(ad)}(u_T)$. This can be understood if the argument is recast in terms of the properties of the (collinear) PES in skewed mass-weighted coordinates. While originally introduced for thermoneutral reactions,[71] this interpretation is particularly suitable for exoergic reactions with an early barrier. Because of the varying width of the exit valley for different isotopes, at high E_T trajectories are increasingly reflected from the repulsive wall back into the reagent valley in the order Mu $\geqslant$ H $\geqslant$ T. The properties of the repulsive wall of the PES are thus also relevant. This behaviour is readily identified in the collinear $X + F_2$ reaction,[72] and has also been observed in the three-dimensional system.[26] The isotope effect in $\sigma_r^{(ad)}(E_T)$ can thus be traced back to the interplay between mass scaling and the accessibility of the exit channel on the PES.

Electronic non-adiabaticity modifies this behaviour for dissociation, but not for reaction. The main reason for the different effects of non-adiabaticity on σ_r and σ_d lies in the different energy domains of the two processes. Reaction proceeds in the lower E_T range, where non-adiabaticity is not very pronounced, *i.e.* $\sigma_{hop} < \sigma_r$, and hence the mechanism of reaction cannot be changed significantly by non-adiabatic effects.

In contrast, the E_T range where dissociation proceeds readily coincides with the range of pronounced non-adiabaticity. At these higher E_T, transitions to excited PESs are frequent. On the excited PESs dissociative forces persist out to large distances, and F_2 can be dissociated even by the light Mu, because the required momentum can be supplied by the repulsive potential. This is an important consideration for high-energy models of dissociation which incorporate simplistic potentials. Such models should be based on suitable diabatic PESs rather than on parameters taken from the adiabatic ground state PES.

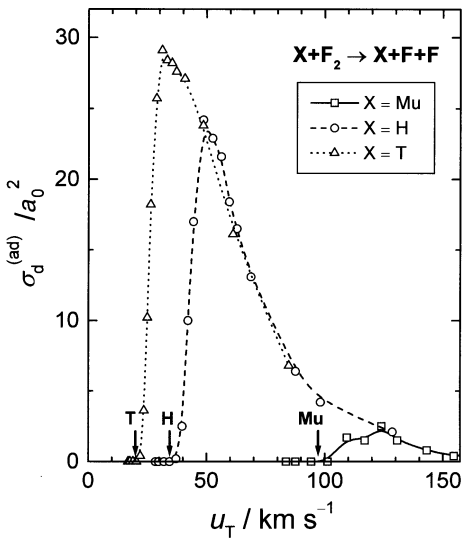

Fig. 8 QCT dissociation cross sections $\sigma_d^{(ad)}$ *vs.* effective translational velocity u_T for $X + F_2$ collision-induced dissociation. (—□—) X = Mu. (– – ○ – –) X = H. (· · △ · ·) X = T. The arrows near the abscissa correspond to collision energies E_T at dissociation threshold.

It should be noted that the potential parameters which determine the behaviour of $X + F_2$ with respect to CID (*e.g.* dissociation energies, repulsive forces and the ranges of the inter- and intramolecular contributions) have typical molecular values. It may then be speculated that the light mass of Mu is essential for opening an E_T-window where the non-adiabatic mechanism of CID is dominant. Indeed, previous investigations of CID in atom–diatom collisions with atoms of 'normal' mass (see *e.g.* an earlier systematic study by Blais *et al.*[73] and a very recent paper by Voronin *et al.*[74]) as well as related studies of diatom–diatom collisions (see Eaker and Schatz[75]) have revealed weak to moderate non-adiabatic enhancement of CID, but no case where the non-adiabatic mechanism is dominant.

D Isotope dependence of non-adiabatic behaviour

The results in Section IV indicate that breakdown of the BO separation and coupling of electronic states play an important role in the post-threshold collision dynamics of $X + F_2$. However, depending on the isotopomer and macroscopic channel, there are considerable variations in the effects of non-adiabaticity on the observable cross sections, ranging from a negligible influence to a complete change in the qualitative characteristics of a given process.

In order to illustrate these variations, we consider the isotopic ratios of σ_{hop} (or σ_{mix} at low E_T) for Mu, H and $T + F_2$. Near threshold ($E_T = 0.5$ eV), the isotopic ratios for σ_{mix} are $\approx 1 : 0.8 : 0.5$, with very large statistical uncertainties. Changing to σ_{hop} in the post-threshold range, the isotopic ratios drop to $\approx 1 : 0.7 : 0.4$ at $E_T = 8$ eV, *i.e.* the isotope effect increases, while the ratios decrease again as E_T is further increased. Finally in the high E_T limit the isotopic ratios appear to level off at $\approx 1 : 0.9 : 0.8$ (values at $E_T = 50$ eV).

An independent estimate of these isotope effects can be obtained from Landau–Zener theory.[15,76,77] We expect[15]

$$P_{hop} = \exp\left(-\frac{\lambda \Delta V}{\hbar u_n}\right) \quad (7)$$

where P_{hop} is the single-passage transition probability between adiabatic potentials at an avoided crossing. In eqn. (7), λ is a characteristic distance over which the adiabatic potentials change substantially, ΔV is the splitting of the adiabatic potential sheets, u_n is an effective average velocity for the nuclear motion, and λ, ΔV, and u_n all depend on the nuclear coordinates. The exponent in eqn. (7) is the Massey parameter γ.[15,78]

For a given trajectory and hopping location, P_{hop} depends only on u_n. Substituting the kinetic energy E_n corresponding to u_n,

$$u_n = (2E_n/\mu_n)^{1/2} \quad (8)$$

where μ_n is an effective reduced mass for the mode of nuclear motion that induces the electronic transition, an explicit mass dependence is introduced into P_{hop},

$$P_{hop} = \exp(-\kappa \mu_n^{1/2}/E_n^{1/2}) \quad (9)$$

Here κ represents the remaining terms from eqn. (7) and (8). Finally, after batch averaging of P_{hop} a convolution of terms of the form of eqn. (9) will appear in σ_{hop}, which results in a complicated direct and indirect isotope dependence.

In general it is not possible to make firm predictions or to understand the isotopic ratios of σ_{hop} at a given E_T on the basis of the above considerations. Two very restrictive conditions have to be fulfilled if eqn. (9) is to be useful: (1) within a

batch, κ as well as E_n should be similar for all trajectories contributing significantly to σ_{hop} (in particular this condition holds if only one type of trajectory is associated with surface hops), and (2) κ and E_n should be the same for different isotopomers.

We now discuss the limiting situations in which these conditions are expected to prevail. The first of them is the threshold E_T range. At low E_T the small value of u_n at the entrance channel barrier, together with the large splitting ΔV means surface hopping at the barrier will be suppressed. Electronic transitions will be confined to the regions of the PESs where the gap between the two lowest adiabatic surface sheets is least and the nuclear motion is fastest. This makes hopping most likely for reactive trajectories as they enter the F + XF exit valley with its asymptotic degeneracy for the two lowest adiabatic potential sheets [compare Fig. 1(b)]. The local nuclear motion during electronic promotion will then correspond to F–XF separation. The reduced masses corresponding to this motion are almost isotopically invariant; $\mu_n = \mu_{F,XF} \approx 0.5 m_F$. Thus no sizeable isotope effect is expected for either P_{hop} or σ_{hop}.

Furthermore, if electronic transitions are confined to reactive trajectories, as is suggested by the above scenario, then the isotope effect in σ_{hop} has to be convoluted with the reaction probabilities. At low E_T these are smallest for Mu and largest for T, which suggests the possibility of an 'inverted' isotope effect. On the other hand, each trajectory's motion towards the exit valley has a component of X–F_2 translation, which will tend to decrease the isotopic ratios, *i.e.* to enhance the isotope effect. Combining all these arguments, at low E_T we expect the isotope effect in σ_{hop} to be weak.

As E_T and u_n increase, and along with them σ_{hop}, the probability for transitions across larger potential gaps also increases. In particular at higher E_T we expect a dominance of transitions at the avoided intersection forming the potential barrier in the entrance channel of the adiabatic ground state PES. The principal nuclear motion for such transitions is X–F_2 translation with an effective mass $\mu_n = \mu_{X,F_2} \approx m_X$. This corresponds to the most pronounced isotopic mass ratios that can be realised in the XF_2 systems. Furthermore, in the entrance channel up to the hopping location at the barrier the trajectories are isotopically nearly invariant, so that at a given E_T, the constants κ and E_n in eqn. (9) are similar within all batches and for all isotopes.

From this behaviour we expect the following trends: (1) at moderate E_T there should be a noticeable isotope effect in the P_{hop} because of the large effective mass ratio, and (2) the isotope effect in σ_{hop} will decrease as E_T increases, and will disappear in the high E_T limit as $P_{hop} \rightarrow 1$.

In the high E_T limit, the σ_{hop} are of the same order of magnitude as the total rearrangement cross section $\sigma_r + \sigma_d$. Hence at high E_T, there is a close connection between strong electronic interaction and strong nuclear interaction. In more detail, almost all high E_T non-adiabatic trajectories are dissociative. With few exceptions, if a trajectory experiences electronic coupling, it will also lead to fragmentation. This is a remarkable situation, since *a priori* we might expect that a fraction of the trajectories producing tight collision complexes would re-emerge inelastically. However, this is not the case, and as is evident from the small values of $\sigma_{hop,i}$ in Fig. 3, inelastic collisions involving surface hops are rare.

Because of the repulsive nature of the excited F_2 states, all inelastic, non-dissociative trajectories must exit on the adiabatic ground state surface, implying that such trajectories must undergo at least one additional surface hop back to the ground state PES. Specifically in the high E_T range these are trajectories at large impact parameters which mark the transition from strong interaction to a fly-by situation. Such trajectories cross the barrier twice in a Landau–Zener double-passage manner. Denoting for the moment the single-passage transition probability of eqn. (9) as P_1, we have for this double-passage, double-hopping situation

$$P_{hop} = P_1^2 = \exp(-2\kappa\mu_n^{1/2}/E_n^{1/2}) \quad (10)$$

Squaring P_1 increases the isotope effects relative to the cases treated by eqn. (9). Furthermore, since large impact parameter inelastic collisions involve mainly X–F_2 relative motion, so that $\mu_n \approx m_X$, the isotope effect in $\sigma_{hop,i}$ is expected to be more pronounced than in the other components and in σ_{hop}. After averaging over the range 10 eV $\leqslant E_T \leqslant$ 20 eV for improved statistical accuracy, $\sigma_{hop,i}$ from the CPSH–PDOT calculations is found to have isotopic ratios of $1 : (0.41 \pm 0.09) : (0.25 \pm 0.07)$, which indeed amounts to the largest isotope effect observed for any of the surface-hop or mixing cross sections.

VI Summary and conclusions

We have found that in the hyperthermal and hot-atom regimes the extent of electronic non-adiabaticity is significant for all isotopomeric X + F_2 systems, as judged by the large values of σ_{hop}. Nevertheless, we expect non-adiabatic effects to be observable mainly in detailed or differential cross sections. Owing to extensive averaging, the effects of non-adiabaticity are less obviously apparent in total cross sections and rate coefficients.

Thus a simple model for X + F_2 reactions is to assume an electronically adiabatic process evolving on the adiabatic ground state PES. However, there are small, but distinctive effects from electronic transitions, which for most realistic conditions tend to reduce the reaction cross sections, rate coefficients and reactivity integrals. Similarly for $E_T \leqslant 20$ eV the T + F_2 dissociation (3b) proceeds efficiently on the lowest PES and the probability of dissociation is hardly affected by electronic transitions.

In marked contrast, a spectacular exception is the huge non-adiabatic effect on the dissociation cross section of Mu + F_2 collisions. Thus contrary to popular models based on electronically adiabatic nuclear motion, even the very light Mu atom can dissociate F_2 efficiently—but only in non-adiabatic collisions. Surface hopping (or another non-adiabatic technique) is essential for describing the dynamics of the Mu + F_2 system and for simulations of Mu hot-atom processes.

This is also true for Mu rate coefficient or yield calculations if very accurate results are required, although the magnitudes of the reaction cross sections are not very sensitive to non-adiabatic processes. The yields in hot-atom systems can be affected by electronic transitions in a number of ways: directly through changes in the reactivity, but also indirectly through non-reactive processes, which change the slowing-down of Mu in the laboratory system. In general these energy transfer processes will be enhanced by the inclusion of non-adiabatic electronic coupling due to the fact that the electronic degree of freedom can absorb additional collision energy. Yet considering all these points it must not be overlooked that a prerequisite for accurate results is the availability of accurate PESs.

In this paper we have confined our discussion to effects which can be analysed using batches of trajectories, *i.e.* cross sections or cross-section-like quantities. A more detailed picture of the non-adiabatic and adiabatic mechanisms emerges from an analysis of individual trajectories. Such an investigation will be presented elsewhere.[40]

Acknowledgements

We thank Dr. R. Polák for making available the F_2 coupling elements, Professor D. G. Fleming for communicating the results of ref. 11, and A. Pokorny and A. Dokalik for computational assistance. We gratefully acknowledge financial

support of this research by the Austrian Science Foundation (FWF) under Grant. No. 09704-CHE and by the UK Engineering and Physical Sciences Research Council.

References

1 T. Tominaga and E. Tachikawa, *Modern Hot Atom Chemistry and Its Applications*, Springer, Berlin, 1981.
2 *Hot Atom Chemistry: Recent Trends and Applications in the Physical and Life Sciences and Technology*, ed. T. Matsuura, Elsevier, Amsterdam, 1984.
3 *Handbook of Hot Atom Chemistry*, ed. J-P. Adloff, P. P. Gaspar, M. Imamura, A. G. Maddock, T. Matsuura, H. Sano and K. Yoshihara, Kodansha, Tokyo, 1992.
4 D. C. Walker, *Muon and Muonium Chemistry*, Cambridge University Press, Cambridge, UK, 1983.
5 D. G. Fleming, M. Senba, D. J. Arseneau, I. D. Reid and D. M. Garner, *Can. J. Chem.*, 1986, **64**, 5.
6 D. G. Fleming, *Radiat. Phys. Chem.*, 1986, **28**, 115.
7 J. R. Kempton, D. J. Arseneau, D. G. Fleming, M. Senba, A. C. Gonzalez, J. J. Pan, A. Tempelmann and D. M. Garner, *J. Phys. Chem.*, 1991, **95**, 7338.
8 M. Senba, D. J. Arseneau and D. G. Fleming, in ref. 3, p. 232.
9 D. J. Malcolme-Lawes, in ref. 2, p. 39.
10 T. Valencich, in ref. 3, p. 188.
11 M. Senba, D. G. Fleming, D. J. Arseneau and H. R. Mayne, personal communication.
12 P. J. Kuntz, in *Modern Theoretical Chemistry*, Vol. 2: *Dynamics of Molecular Collisions*, Part B, ed. W. H. Miller, Plenum, New York, 1976, p. 53.
13 Z. B. Alfassi and M. Baer, *Chem. Phys.*, 1981, **63**, 275.
14 E. A. Gislason and M. Sizun, *Chem. Phys.*, 1989, **133**, 237.
15 E. E. Nikitin, *Theory of Elementary Atomic and Molecular Processes in Gases*, translated from the Russian by M. J. Kearsley, Clarendon, Oxford, 1974.
16 J. C. Tully, *Faraday Discuss.*, 1998, **110**, 407.
17 J. C. Tully, in *Modern Methods for Multidimensional Dynamics Computations in Chemistry*, ed. D. L. Thompson, World Scientific, Singapore, 1998, p. 34.
18 G. D. Billing, *Int. Rev. Phys. Chem.*, 1994, **13**, 309.
19 D. M. Garner, D. G. Fleming and J. H. Brewer, *Chem. Phys. Lett.*, 1978, **55**, 163.
20 A. C. Gonzalez, I. D. Reid, D. M. Garner, M. Senba, D. G. Fleming, D. J. Arseneau and J. R. Kempton, *J. Chem. Phys.*, 1989, **91**, 6164.
21 D. G. Fleming and M. Senba, in *Perspectives of Meson Science*, ed. T. Yamazaki, K. Nakai and K. Nagamine, Elsevier, Amsterdam, 1992, p. 219.
22 K. H. Homann, H. Schweinfurth and J. Warnatz, *Ber. Bunsen-Ges. Phys. Chem.*, 1977, **81**, 724.
23 N. Jonathan, S. Okuda and D. Timlin, *Mol. Phys.*, 1972, **24**, 1143; *erratum*, *ibid.*, 1973, **85**, 496.
24 J. C. Polanyi, J. J. Sloan and J. Wanner, *Chem. Phys.*, 1976, **13**, 1.
25 L. S. Dzelzkalns and F. Kaufman, *J. Chem. Phys.*, 1982, **77**, 3508.
26 J. N. L. Connor, A. Laganà, A. F. Turfa and J. C. Whitehead, *J. Chem. Phys.*, 1981, **75**, 3301.
27 R. Steckler, D. G. Truhlar and B. C. Garrett, *Int. J. Quantum Chem. Symp.*, 1986, **20**, 495.
28 B. C. Garrett, R. Steckler and D. G. Truhlar, *Hyperfine Interact.*, 1986, **32**, 779.
29 D. C. Clary and J. N. L. Connor, *J. Chem. Phys.*, 1981, **75**, 3329.
30 F. O. Ellison, *J. Am. Chem. Soc.*, 1963, **85**, 3540.
31 P. J. Kuntz, in *Theoretical Models of Chemical Bonding, Part 2: The Concept of the Chemical Bond*, ed. Z. B. Maksić, Springer, Berlin, 1990, p. 321.
32 W. Jakubetz and P. J. Kuntz, *Chem. Phys.*, 1994, **179**, 241.
33 D. G. Truhlar and C. J. Horowitz, *J. Chem. Phys.*, 1978, **68**, 2466; *erratum*, *ibid.*, 1979, **71**, 1514.
34 A. J. C. Varandas, F. B. Brown, C. A. Mead, D. G. Truhlar and N. C. Blais, *J. Chem. Phys.*, 1987, **86**, 6258.
35 A. I. Boothroyd, W. J. Keogh, P. G. Martin and M. R. Peterson, *J. Chem. Phys.*, 1996, **104**, 7139.
36 P. J. Kuntz, *J. Chem. Phys.*, 1991, **95**, 141.
37 M. Amarouche, F. X. Gadéa and J. Durup, *Chem. Phys.*, 1989, **130**, 145.
38 F. X. Gadéa and M. Amarouche, *Chem. Phys.*, 1990, **140**, 385.
39 D. G. Truhlar and J. T. Muckerman, in *Atom–Molecule Collision Theory—A Guide for the Experimentalist*, ed. R. B. Bernstein, Plenum, New York, 1979, p. 505.
40 W. Jakubetz and P. J. Kuntz, to be published.
41 J. J. Duggan and R. Grice, *J. Chem. Phys.*, 1983, **78**, 3842.
42 R. Polák, personal communication.
43 R. Polák, J. Vojtík and F. Schneider, *Chem. Phys. Lett.*, 1982, **85**, 107.
44 R. Polák and P. J. Kuntz, *Chem. Phys.*, 1992, **168**, 301.
45 G. Herzberg and H. C. Longuet-Higgins, *Discuss. Faraday Soc.*, 1963, **35**, 77.
46 G. J. Atchity, S. S. Xantheas and K. Ruedenberg, *J. Chem. Phys.*, 1991, **95**, 1862.
47 I. Last and M. Baer, *J. Chem. Phys.*, 1984, **80**, 3246.
48 P. B. Benneyworth, G. G. Balint-Kurti, M. J. Davis and I. H. Williams, *J. Phys. Chem.*, 1992, **96**, 4346.
49 G. L. Fox and H. B. Schlegel, *J. Am. Chem. Soc.*, 1993, **115**, 6870.
50 T. Takayanagi and Y. Kurosaki, *J. Phys. Chem. A*, 1997, **101**, 7098.
51 M. Bittererová, S. Biskupic, H. Lischka and W. Jakubetz, in preparation.
52 P. J. Kuntz, B. I. Niefer and J. J. Sloan, *J. Chem. Phys.*, 1988, **88**, 3629.
53 P. J. Kuntz, in *Selectivity in Chemical Reactions. Proceedings of the NATO Advanced Research Workshop on Selectivity in Chemical Reactions*, Bowness-on-Windermere, UK, 7–11 September 1987, ed. J. C. Whitehead, Kluwer, Dordrecht, 1988, p. 403.
54 G. D. Billing, *Chem. Phys.*, 1975, **9**, 359.
55 S. C. Mehrotra and J. E. Boggs, *J. Chem. Phys.*, 1975, **63**, 4618.
56 K. J. McCann and M. R. Flannery, *J. Chem. Phys.*, 1975, **63**, 4695.
57 D. J. Diestler, *J. Chem. Phys.*, 1983, **78**, 2240.
58 L. L. Halcomb and D. J. Diestler, *J. Chem. Phys.*, 1986, **84**, 3130.
59 W. H. Miller and C. W. McCurdy, *J. Chem. Phys.*, 1978, **69**, 5163.
60 H-D. Meyer and W. H. Miller, *J. Chem. Phys.*, 1979, **70**, 3214.
61 A. Bjerre and E. E. Nikitin, *Chem. Phys. Lett.*, 1967, **1**, 179.
62 J. C. Tully and R. K. Preston, *J. Chem. Phys.*, 1971, **55**, 562.
63 N. C. Blais and D. G. Truhlar, *J. Chem. Phys.*, 1983, **79**, 1334.
64 G. Parlant and E. A. Gislason, *J. Chem. Phys.*, 1989, **91**, 4416.
65 J. C. Tully, *J. Chem. Phys.*, 1990, **93**, 1061.
66 M. F. Herman, *J. Chem. Phys.*, 1984, **81**, 754.
67 J. C. Tully, *J. Chem. Phys.*, 1974, **60**, 3042.
68 J. Durup, *Chem. Phys. Lett.*, 1986, **132**, 299.
69 S. Hammes-Schiffer and J. C. Tully, *J. Chem. Phys.*, 1994, **101**, 4657.
70 R. Wolfgang, *Prog. React. Kinet.*, 1965, **3**, 97.
71 B. A. Hodgson and J. C. Polanyi, *J. Chem. Phys.*, 1971, **55**, 4745.
72 J. N. L. Connor and A. Laganà, *Mol. Phys.*, 1979, **38**, 657.
73 N. C. Blais, D. G. Truhlar and C. A. Mead, *J. Chem. Phys.*, 1988, **89**, 6204.
74 A. I. Voronin, J. M. C. Marques and A. J. C. Varandas, *J. Phys. Chem. A*, 1998, **102**, 6057.
75 C. W. Eaker and G. C. Schatz, *J. Chem. Phys.*, 1988, **89**, 6713.
76 L. D. Landau, *Phys. Z. Sowjetunion*, 1932, **2**, 46; reprinted in *Collected Papers of L. D. Landau*, ed. and with an introduction by D. Ter Haar, Pergamon, Oxford, 1965, p. 63.
77 C. Zener, *Proc. R. Soc. London, Ser. A*, 1932, **137**, 696.
78 H. S. W. Massey, *Rep. Prog. Phys.*, 1949, **12**, 248.

Paper 8/08181F